



HAL
open science

A global approach for a consistent identification of static and dynamic phenomena in a PEM Fuel Cell

S. El Aabid, Jérémi Regnier, Christophe Turpin, O. Rallières, E. Soyez, N. Chadourne, J. D'arbigny, T. Hordé, E. Foch

► To cite this version:

S. El Aabid, Jérémi Regnier, Christophe Turpin, O. Rallières, E. Soyez, et al.. A global approach for a consistent identification of static and dynamic phenomena in a PEM Fuel Cell. *Mathematics and Computers in Simulation*, 2019, 158, pp.432-452. 10.1016/j.matcom.2018.10.008 . hal-02412673

HAL Id: hal-02412673

<https://hal.science/hal-02412673>

Submitted on 21 Oct 2021

HAL is a multi-disciplinary open access archive for the deposit and dissemination of scientific research documents, whether they are published or not. The documents may come from teaching and research institutions in France or abroad, or from public or private research centers.

L'archive ouverte pluridisciplinaire **HAL**, est destinée au dépôt et à la diffusion de documents scientifiques de niveau recherche, publiés ou non, émanant des établissements d'enseignement et de recherche français ou étrangers, des laboratoires publics ou privés.



Distributed under a Creative Commons Attribution - NonCommercial 4.0 International License

A global approach for a consistent identification of static and dynamic phenomena in a PEM Fuel Cell

S. El Aabid^{a, b}, J. Regnier^b, C. Turpin^b, O. Rallières^b, E. Soyez^a, N. Chadourne^a,
J. d'Arbigny^c, T. Hordé^d, E. Foch^e

^aInstitute of Technology IRT Saint Exupéry, More Electric Aircraft Department, F-31432 Toulouse, France

^bLAPLACE, Université de Toulouse, CNRS, INPT, UPS, F-31071 Toulouse, France

^cZodiac Aerotechnics, F-78370 Plaisir, France

^dSafran Power Units, F-31019 Toulouse, France

^eAirbus Group, F-31707 Blagnac, France

Abstract

In this paper, we propose a parameterization process for static and dynamics models dedicated to the analysis of two typical characterizations of a Proton Exchange Membrane Fuel Cell (PEMFC): the polarization curve (V-I curve) and a set of Electrochemical Impedance Spectroscopies (EIS) carried out for several current densities of this curve. The specificity of the proposed approach is to consider **conjointly** both characterizations during all the proposed analysis process. This global strategy ensures the separation of the different fuel cell phenomena (activation, diffusion and ohmic) in the static and dynamic domains by imposing, with different ways, an expected consistency between both characterizations.

Starting from the measured polarization curve, a first parametric identification is carried out leading to a static model of the Fuel Cell (FC). The EIS data are, at this stage, used to obtain the ohmic resistance of the static model. This is the first consistency forced between both characterizations. By fixing the transfer coefficient to 0.5 (platinum catalysts), it is possible to separate unequivocally the different fuel cell phenomena (activation, diffusion and ohmic) and to identify the different parameters of the laws which describe them in steady state for a given Membrane Electrode Assembly (MEA).

In the objective of describing the dynamic of these three phenomena, an identification process for generic models involving RC cells in series and without *a priori* (number of RC cells not presupposed) is secondly applied to the set of measured EIS. Thanks to time-constant spectra (not classically used in fuel cell world) handled in this approach, the time-constants related to the three phenomena are extracted. The first specificity is to force the consistency between V-I curve and EIS by calculating the activation and diffusion resistances thanks to the derivation of the physical laws used for the static model and parameterized in the first step of our approach. The second specificity consists in forcing the equality between the V-I slope and the “zero-frequency resistor” of the EIS for a given characterized density current. This results in the apparition of a residual part for the impedance involving different suffered phenomena (potentially platinum oxidation, channel pressure oscillations...). The characteristics of this residue are analyzed.

To calibrate the **proposed** method and to **demonstrate** its sensitivity to changes that may occur in the FC components, experiments concerning a single cell with different sets of components (different membrane thicknesses and different platinum loadings in the Active Layer (AL)) were achieved and analyzed by applying this method. **Cyclic voltammetries** were carried out in addition of V-I curves and EIS to check the relevancy of the parameters identified through our approach.

Keywords: PEM fuel cell, polarization curve, Electrochemical Impedance Spectroscopy (EIS), consistent static and dynamic modelling, time-constant spectra.

1. Introduction

One of the most abundant resources on earth is hydrogen covering the most of the earth area in the form of water, making it one of the main energy vectors of tomorrow. Moreover, the high energy density of hydrogen makes it a potential candidate for the future of the energy storage.

The Proton Exchange Membrane Fuel Cell (PEMFC) is a mature component to generate, from hydrogen, electricity (and heat). This device is characterized by a good efficiency of conversion to electrical energy. Thus, it is potentially an effective way of decreasing pollutant emissions if hydrogen is produced in a green way (typically from renewable energies).

Despite the certain maturity of fuel cells, their ageing remains to be understood and improved especially in the aeronautical applications (general framework of our study) where feedback is much lower than for automotive applications for example. Hence, there is still a need to continue developing methods dedicated to monitor the fuel cell ageing during all these developments even more beyond. The present paper is a contribution in this framework.

The ageing monitoring of fuel cells relies on several tools including typically the polarization curve (V-I curve) and the electrochemical impedance spectroscopy (EIS). However, if the use of the EIS is relatively well controlled to diagnose fuel cell flooding, drying, tracking internal resistance value [1] [2] or hydrogen leakage [3] [4], the exploitation and interpretation of the impedance spectra is still more generally an issue (no clear consensus), even if it could appear amazing.

Faced to this situation, the proposed methodology by the authors in the present paper is especially to overcome a recurrent experimental observation made by the daily users of EIS: there is a not-clearly explained difference between the low frequency resistance (some tens of $m\Omega$ to some hundreds of $m\Omega$ typically) of the EIS and the slope of the polarization curve for a given current density. Theoretically the two quantities have to tend towards the same value. In others words, a part of the impedance spectra is not clearly and easily exploitable to characterize fuel cell performance. This topic has been discussed in the literature in the last years. A variety of tracks has been proposed to explain the fuel cell behavior at low frequency.

Before to describe the tracks found in literature, let us underline that the understanding difficulty is reinforced by the regular instability of measurements in this frequency range. It is now clear that the low frequency current oscillations imposed during the EIS create oxygen-pressure oscillations within the cathode gas channels (to a lesser extent for the hydrogen side), difficult to compensate with classical gas control command. This affects thus the local impedance along the channels and by this the overall impedance response of the fuel cell. In other words, the EIS becomes intrusive concerning the fuel cell operation, which is clearly not desired.

In that way, the difference between the low frequency limit of the impedance and the slope of the polarization curve has been analyzed in [5]. The authors demonstrate that a relation linking the two resistances' difference with the cathode stoichiometry can be obtained. It is shown also in [6] that the amplitude of the oxygen concentration oscillation, created as a consequence of ac current at the electrode, extends into the gas channels below frequencies of 10 Hz.

Several explanations were moreover oriented to the platinum oxidation or the formation of hydrogen peroxide that could have an impact at low frequency. In [7], a low-frequency inductive loop was observed in the impedance measurements of a single-cell PEM fuel cell.

This loop was observed for all current densities along the polarization curve. The authors developed analytic models accounting formation of hydrogen peroxide and formation of PtO as a consequent of dissolution of Pt; these models allow to predict the fuel cell behavior at low frequency.

Taking into account the overlap of several phenomena and the fact that their impacts are not yet clearly established, the classical approaches with presupposed models appears not well adapted to analyze the impedance spectra issued from EIS. Approaches without *a priori* seem unavoidable. In this way, this paper proposes to use a not-usual point of view in the fuel cell world: the time-constant spectra which can be obtained also from EIS. Based on the fact that a lot of physical phenomena have a first-order behavior in first approximation, this method searches all the time-constants contained in EIS measurements via a theoretically-infinite network of RC in series. The final result is given with a time-constant spectrum. These time-constant spectra are characterized by a set of time constants $\tau_i=R_iC_i$ and the magnitude of their resistances R_i . This method was recently described in [8].

This method has been used in [8] to extract time-constant spectra from the fuel cell voltage response to small current steps in the objective of diagnosing flooding. An exploitation of the distribution of relaxation times to diagnose cells polarity reversal by insufficient hydrogen supply was treated in [9]. The method has been also exploited for thermal diagnosis of power electrical components by Szekely et al. [10] [11] [12], illustrating the general nature of this approach.

In the present paper and in an original way, the authors propose to introduce physical meaning to this general approach by introducing physical laws related to activation and diffusion phenomena. By this way, the objective is to reveal the signature of other phenomena (potentially gas-concentration oscillations, platinum oxidation...).

In this global context of difficulty to interpret the performance of a fuel cell through its polarization curve and several EIS measured along this curve, the authors of the present paper propose a global approach to interpret with a maximum of consistency these two kinds of characterization. Concretely this interpretation is achieved through two models, respectively for static conditions (V-I curve) and small-amplitude dynamic conditions (EIS) by ensuring the consistency between the static behavior and the dynamic behavior. This consistency is ensured by introducing into each parametrization process (one for the static model, one for the dynamic model) parameters and/or laws from the other part and by forcing the convergence between two models at low frequency (see Fig. 1).

With this approach, the reader will be able to see how the authors quantify the classical phenomena (activation, diffusion, ohmic) and how they reveal a residual part (not specifically attributed to such or such phenomenon, even if tracks of explanation are proposed) in the case of the modelling of the dynamic behavior. *In fine*, the objectives of the authors are indeed clearly to separate and quantify each involved phenomenon with a robust method and to be able in the future to follow an ageing of a fuel cell through the time evolution of each phenomenon.

Before applying this method to ageing monitoring, the authors applied it to healthy components. It was indeed necessary to “calibrate” the proposed method regarding its relative complexity and to demonstrate its sensitivity to changes (here supposed mastered) that may occur in a fuel cell. In this way, experiments with a single cell (PEMFC) with different sets of internal components (different membrane thicknesses and different platinum loadings in the Active Layer (AL)) were achieved and analyzed by applying the proposed method. Cyclic voltammetries were carried out in addition of V-I curves and EIS to check the relevancy of the parameters identified through our approach.

The first and following part will describe the used fuel cell and the three tested different Membrane Electrode Assemblies (MEAs) with supposed known characteristics. The second part will deal with the static model and the proposed parameterization process. The third part will present the dynamic model and the proposed parameterization process based on the method of the time-constant spectra. All along this paper, the reader has to keep in mind the interleaving/coupling of both processes which will be underlined whenever possible.

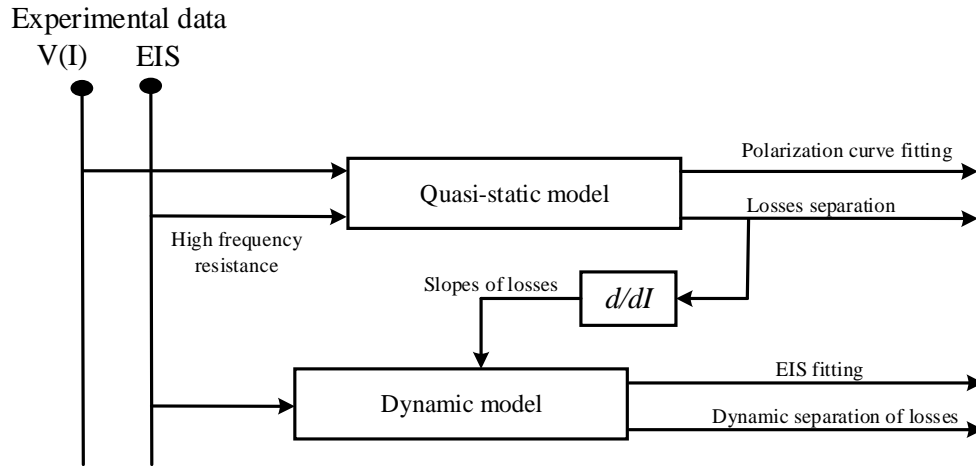


Fig. 1. The identification process of both quasi-static and dynamic models

2. Experimental setup

The methods developed in this paper were applied to a single PEM cell with an active electrode area of 50 cm^2 ($71 \times 71 \text{ mm}$) made up of aluminum clamp plates, copper electronic collectors, graphite plates engraved with $1 \times 1 \text{ mm}$ gas distribution channels and O-ring grooves. The heating of the cell is carried out by resistances inserted in the clamp plates. A photograph of the cell is shown in Fig. 2.



Fig. 2. The single cell used in this study [13]

The study concerned 3 MEAs with different membranes thicknesses and platinum loadings, the platinum being the material used to catalyst the electrochemical reactions in PEM fuel cells. The features of each MEA are shown in Table 1.

MEA number	Membrane thickness(μm)	Platinum loading anode/cathode ($\text{mg}_{\text{Pt}}/\text{cm}^2$)
MEA 1 (N212 ¹)	50	0.5/0.5
MEA 2 (N212 ¹)	50	0.15/0.25
MEA 3 (NXL ²)	27	0.5/0.5

Table 1. Features of tested MEAs

After the break-in phase and sealing tests of the MEAs, two characterizations are essential to build our models: the polarization curve (Fig. 3) and the EIS (Fig. 8).

¹ N212: Nafion non-reinforced membrane, having a thickness of $50 \mu\text{m}$.

² NXL: Nafion XL, an extended-life reinforced membrane that combines the advantages of mechanical reinforcement with enhanced chemical stability enabling improved membrane durability.

3. Parametric identification based on the polarization curve

3.1. Experimental procedure

The parameterization of the quasi-static model will be performed for each MEA from each polarization curve measured. These curves show the evolution of the voltage V as a function of the current I . The polarization curves corresponding to MEA 1, MEA 2, and MEA 3 are shown in Fig. 3. Each polarization curve was made of 23 steps of current from 0 A to 60 A. A stabilization of one minute was made on each step before taking the measurements.

In this approach, all our tests were achieved with pure H_2 and O_2 to simplify the implementation of the fuel cell, our objective remaining to validate our global methodology. Knowing that the oscillations due to the channels' impedance is limited when using H_2/O_2 [14], the use of H_2/O_2 can offer an opportunity to analyse low frequency phenomena with supposed limited perturbations.

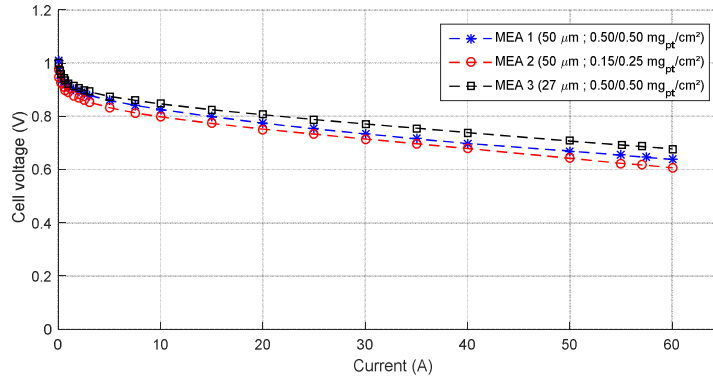


Fig. 3. Polarization curves corresponding to the three MEAs. $T = 80^\circ C$, $P_{H_2/O_2} = 2.5/2.5bar$, stoichiometries H_2/O_2 1.2/1.4, $HR_{H_2/O_2} = 100\%/100\%$

The ohmic resistance R_{ohm} related to each MEA can be isolated thanks to high frequency signals. Using the EIS, these resistances can be calculated from the intersection of the impedance Nyquist plot with the real axis at high frequencies [15] [16]. R_{ohm} is related to the transport of protons in the membrane and the electrons in the electrodes and the other parts of the fuel cell; it also takes into account the ohmic losses due to contact surfaces between internal components in a MEA.

From the spectra of the Fig. 8, the three ohmic resistances were calculated by averaging all the values of the ohmic resistances obtained by the spectrum related to each current. This resistance is given in Table 2 as a function of the number of the MEA.

MEA number	Ohmic resistance R_{ohm} (Ω)	Estimated membrane conductivity ³ (mS/cm)
MEA 1 – 50 μm	0.00136	73.5
MEA 2 – 50 μm	0.00146	68.5
MEA 3 – 27 μm	0.00118	47.5

Table 2. Measured ohmic resistance and estimated conductivity of each MEA,

$$HR_{H_2/O_2} = 100\% / 100\%, T = 80^\circ C$$

As the membranes of the MEAs 1 and 2 are from the same material and have the same thickness, they are supposed to have the same ohmic resistance. The difference (7.3 %) in terms of ohmic resistance between these two MEAs can be explained by the assembly, the clamping, the MEAs manufacture and the break-in phase.

Knowing that MEA 3 has the smallest membrane thickness (almost one half of the other MEAs thicknesses), its ohmic resistance value was expected to be nearly divided by 2 compared to that of the other MEAs. The fact that the ohmic resistance of MEA 3 does not match up with our expectations is explained by the lower conductivity of the mechanically reinforced membrane, as the mechanical reinforcement material is not as effective as the membrane material for proton conductivity.

In terms of performance assessment between the 3 MEAs, it is clearly noticeable that the MEA 3 shows the best performance (Fig. 3) due to two reasons:

- Its small value of ohmic losses (directly related to R_{ohm}).
- Its platinum loading value (0.5/0.5 mg_{pt}/cm^2), which is the highest one with that of MEA 1, allowing consequently to have more reduced activation losses.

3.2. Description of the polarization curve based model

The Fuel Cell voltage V_{FC} in quasi static mode can be expressed as a function of the average current I by the following equation:

$$V_{FC} = E_{Th} - \eta_{ohm} - \eta_{Act} - \eta_{Diff} \quad \text{Eq. 1}$$

Where E_{Th} is the fuel cell theoretical maximum voltage; it depends on the temperature and the

$$E_{Th} = E_{Th}^0 + \frac{R.T}{n.F} \cdot \ln\left(\frac{p_{H_2} \cdot (p_{O_2})^{1/2}}{p_{H_2O}}\right) \quad \text{Eq. 2}$$

gas pressures (Nernst's law):

Where:

E_{Th}^0 : theoretical voltage in standard conditions of temperature and pressure (25 °C, 1 bar). It's equal to 1.23 V.

p_{H_2} : partial pressure of hydrogen, bar

³ To calculate the conductivity of the membrane, we took the assumptions that the resistance of the membrane R_{mem} can be approximated to R_{ohm} (seeing that the resistance due to contact surfaces, electrodes and other parts can be neglected), and the thickness of the membrane doesn't depend on the relative humidity.

p_{O_2} : partial pressure of oxygen, *bar*

p_{H_2O} : partial pressure of water vapor, *bar*

F : Faraday constant, 96485 *C/mol*

n : number of electrons in the reaction (2)

R : universal gas constant, 8.314 *J/K/mol*

T : temperature, *K*

η_{Ohm} , η_{Act} , η_{Diff} are respectively the voltage drops associated to ohmic, chemical activation, and gas diffusion phenomena.

This part of the work is based on an established model in the Laplace laboratory [16], **but very close to the other published ones**. The general form of the model fits large current signals in quasi static mode and describes the different phenomena involved in the fuel cell making it possible to reconstruct the different voltage drops. This model has been used in [17] to describe the evolution of the polarization curve when the operating conditions change using physical laws for each parameter of the model according to the operating conditions.

Ohmic losses are generally assimilated, in terms of interpretation, to the membrane resistance supposed to be widely majority. However, in our case, R_{ohm} is directly measured by EIS without interpretation assumptions:

$$\eta_{Ohm} = R_{Ohm} I \quad \text{Eq. 3}$$

This is the first consistency forced between both characterizations: V-I curve and EIS.

The activation losses are issued from kinetic laws (**Tafel assumption**):

$$\eta_{Act} = \frac{R.T}{\alpha.n.F} \cdot \ln\left(\frac{I + I_n}{I_0}\right) \quad \text{Eq. 4}$$

The diffusion losses are given by the formula:

$$\eta_{Diff} = -\frac{R.T}{\beta.n.F} \cdot \ln\left(1 - \frac{I}{I_{lim}}\right) \quad \text{Eq. 5}$$

Where:

I : operating current, *A*

I_0 : activation current, *A*

I_{lim} : limit current, *A*

I_n : the current representing the gas leakage within the membrane, *A*

α : charge transfer coefficient, in accordance with many bibliographic studies [18] [19], the charge transfer coefficient of the fuel cell in this paper was assumed constant with current, invariant with the operating conditions and equal to 0.5.

β : coefficient representing diffusive phenomena.

3.3. $V(I)$ model identification

The parameterization of the static model was performed from each corresponding polarization curve (three MEAs tested) to separate and quantify each loss for each MEA. The resulting identification problem uses the following parameters' vector:

$$\theta = [I_n; I_0; \beta; I_{lim}] \quad \text{Eq. 6}$$

The model identification comes down to the formulation of an optimization problem which objective function is constituted by a quadratic error criterion J_θ . The aim is to minimize this criterion resulting from the square sum of an error depicting the difference between the voltage given by the model V_{model} and the measured fuel cell voltage V_{exp} as expressed in the Eq. 7.

$$\min[J_\theta] = \min[\sum (V_{model}(\theta) - V_{exp})^2] \quad \text{Eq. 7}$$

The quality of a **parameterization** process lies in the reproducibility of the obtained set of parameters and its ability to reproduce as close as possible the experimental data with a small relative error.

Using the value of R_{ohm} via the EIS (**first consistency forced between V-I curve and EIS**), an optimal set of parameters of the vector θ is identified for each MEA as shown in Table 3. The reproducibility of these results is perfect even with a lot of very different initial conditions. According to us, that is mainly due to the fact to fix the parameter α to 0.5.

Parameters	MEA 1	MEA 2	MEA 3
β	0.0077	0.099	0.29
I_n (A)	0.0616 (1.2 mA/cm ²)	0.066 (1.3 mA/cm ²)	0.108 (2.2 mA/cm ²)
I_0 (A)	$8.33 \cdot 10^{-5}$ ($1.66 \cdot 10^{-3}$ mA/cm ²)	$3.97 \cdot 10^{-5}$ ($7.94 \cdot 10^{-4}$ mA/cm ²)	$1.34 \cdot 10^{-4}$ ($2.68 \cdot 10^{-3}$ mA/cm ²)
I_{lim} (A)	1610 (32.2 A/cm ²)	154.85 (3.09 A/cm ²)	86.72 (1.73 A/cm ²)
$\beta \cdot I_{lim}$ (A)	12.4	15.33	25.15
Max error (%)	0.86	0.2	0.39

Table 3. Parameters' identification of each MEA ($\alpha=0.5$ by assumption)

An example (MEA 2) of the **parameterization** results is shown in Fig. 4.a with the corresponding relative error in Fig. 4.b.

(a)

(b)

Fig. 4. (a) Model fitting of the polarization curve experimental data, and (b) the relative error depicting the difference between the model and experimental data applied to MEA 2.

The relevant comment is that the polarization curves are accurately identified with a maximal error between the model and the measurements less than 1 % for all MEAs, and a high stability of identified parameters thanks to the assumption $\alpha=0.5$.

3.4. $V(I)$ model exploitation

The related losses to each MEA are shown in Fig. 5.

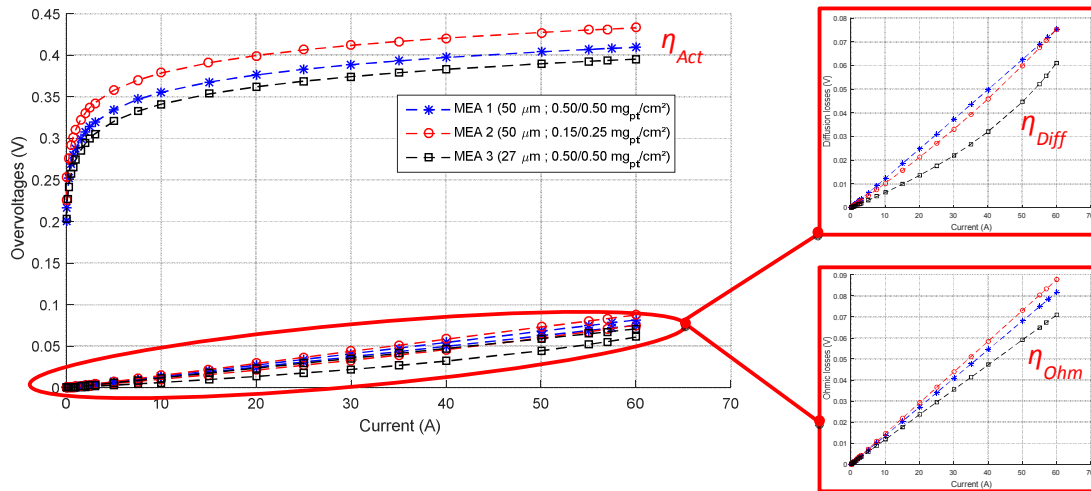


Fig. 5. Voltage drops estimation associated to the main phenomena for each MEA

Since channels and Gas Diffusion Layers (GDLs) are the same for all the MEAs, diffusion losses should be similar for all the MEAs. Small variations can be observed, especially at high currents. They can be due to the slightly different water states within each MEA, the applied break-in supposed identical and not specific to each MEA and the clamping which is the same for all the MEAs even if they don't have the same thicknesses. We notice also that diffusion

losses of MEA 1 are almost linear, that fact explains the high value of its identified limit current I_{lim} (see Table 3).

Concerning the activation phenomena, Fig. 5 shows that MEA 1 and MEA 3 have fewer activation losses due to their platinum loadings that are relatively high compared to MEA 2.

MEA 1 and MEA 3 are supposed to have the same platinum loadings. The difference in terms of activation losses between MEA 1 and MEA 3 is mainly modelled here through the identified I_0 which is higher for MEA 3 compared to MEA 1.

This trend is also confirmed by the variation of the Electrochemical Active Surface area (EAS) (Fig. 6.a) estimated by Cyclic Voltammetry (CV) [20] [21] [22]. The EAS is expressed in cm^2 of platinum per cm^2 , which represents the real used platinum surface. EAS is proportional to the integral of current with respect to time under the peak of anodic scanning obtained by CV (blue area of the example in bottom left of the Fig. 7). Fig. 7 shows also cyclic voltammetry curves with a voltage scan rate of 10 mV/s for each MEA.

According to us, the difference in terms of EAS for MEA 1 and MEA 3 can be probably attributable to the interfaces membrane/ Active Layer (AL) that are different given that the materials of the membranes are different.

The cyclic voltammetry leads also to determine the parameter I_n [20]. This parameter depends on the thickness of the membrane, that justifies its high value for the MEA 3 compared to the other MEAs (Table 3) having the same thickness so almost the same I_n expected. The obtained values of I_n via the voltammetry method underline this trend (Fig. 6.b).

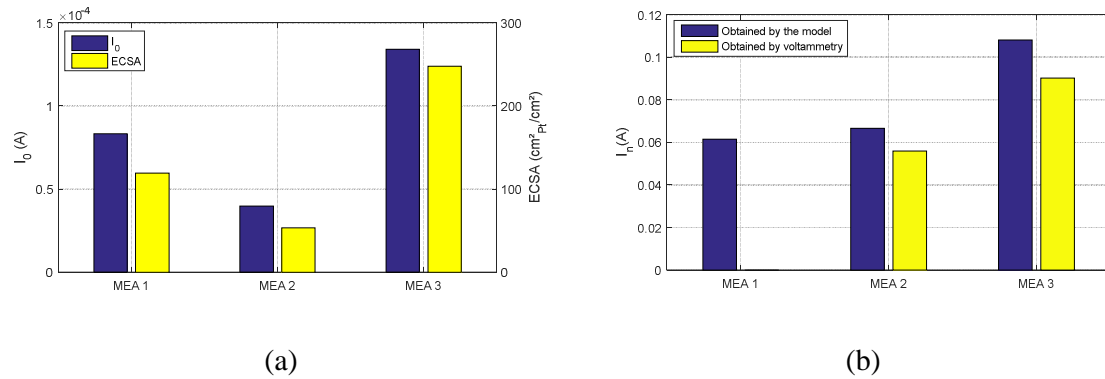


Fig. 6. Comparative of (a) I_0 and (b) I_n for each MEA obtained by two ways (modelling of the V(I) curve and cyclic voltammetry)

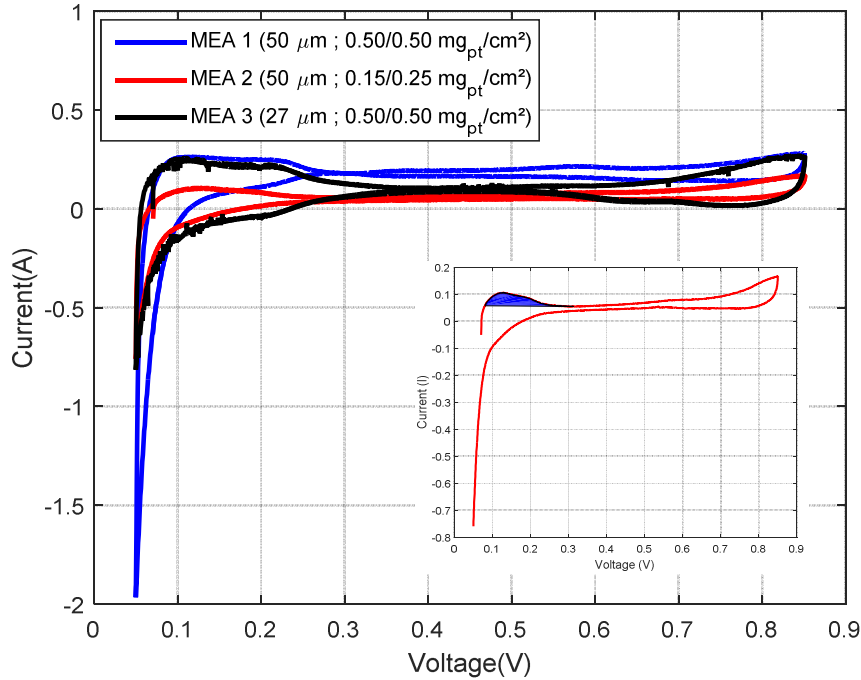


Fig. 7. Cyclic voltammety curves with a voltage scan rate of 10 mV/s for each MEA, and an example applied to MEA 2 showing the scanned area to calculate the EAS

The values for I_0 and I_n are very consistent in terms of evolution for both ways used to estimate them: modelling of the V(I) curve and Cyclic Voltammety. According to us, the key is probably due to the fact to fix the parameter $\alpha=0.5$.

At this step, we can conclude that these results are encouraging for the following of the SoH of a fuel cell. Thanks to the quasi static model based on the measurement of the polarization curve and EIS to estimate R_{ohm} (ensuring a first consistency forced between V-I curve and EIS), and by assuming that the parameter $\alpha=0.5$, it could be possible to characterize the performance of the fuel cell and to evaluate the contribution of the various losses at each operating point. Moreover, tracking them over time could be possible under these conditions. Indeed, different MEAs with different properties, particularly with different platinum loadings, can be seen as a first way to emulate a time evolution of properties due to ageing.

4. Dynamic model for identification from EIS

4.1. Experimental measurements

Although the polarization curve provides useful indicators of overall fuel cell performance, it does not include by principle a dynamic view of the involved phenomena that can give additional information about the fuel cell state of health.

Therefore, in addition to the polarization curve, electrochemical impedance spectroscopies (EIS) were performed for several polarization currents for each MEA. In the previous parts, they were exploited only to estimate the ohmic resistance (ensuring a first consistency forced between V-I curve and EIS). In the following, the aim is to exploit them more deeply.

As the operating point around which the impedance spectroscopy is performed may not remain stable, the interleaved spectroscopy method has been used [15]. The highest frequency

in our case is 50 kHz and the low frequency is in the order of 100 mHz to have a good compromise between the precision and the duration of the procedure.

The Fig. 8 represents the results of the EIS experimental data for MEA 1, 2 and 3 using a range of currents varying from 50 A to 3 A . The number of EIS for each MEA is $N_{EIS} = 10$. A stabilization of one minute was made on each step before taking EIS measurements. We can firstly observe that the spectra for the three MEAs have classical general shapes. Secondly, they are globally close in terms of orders of magnitude, but are significantly different if observed in details. This is rather amazing: particularly, we would expect spectra close for MEA 1 and MEA 3 whereas the closest spectra are for the MEA 2 and the MEA 3. The links between the properties of the three MEAs and the impedance spectra are not so obvious than the ones expected and globally obtained for the polarization curves. A complexity thus appears from the observation of the obtained impedance spectra.

The following proposes a path to analyze these measured spectra for the three MEAs by using the polarization curve modelling and the concept of time-constant spectra.

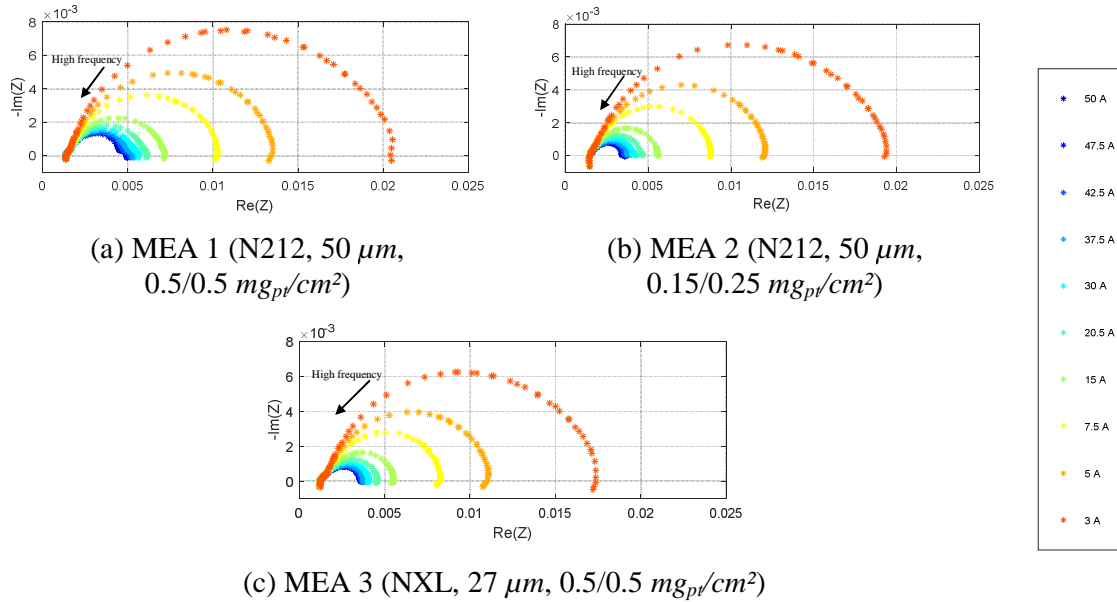


Fig. 8. Impedance spectra for several values of currents for MEA 1, MEA 2 and MEA 3. $T = 80^\circ\text{C}$, $P_{H_2/O_2} = 2.5/2.5 \text{ bar}$, stoichiometries $H_2/O_2 = 1.2 / 1.4$, $HR_{H_2/O_2} = 100\% / 100\%$

4.2. Consistency between quasi static and dynamic measurements

In this work, a particular interest was paid to ensure consistency between quasi static and dynamic measurements. It seems obvious to ensure such a consistency, but we can see that few studies try to do that.

More exactly, it is about to ensure the coherence between the slope of the polarization curve and the very low frequency impedance values of EIS. Indeed, by principle, the EIS aims to study the variation of the fuel cell voltage around a given fuel cell current. Theoretically, the impedance values of EIS must thus converge towards the slope of the polarization curve as the frequency tends to zero.

This consistency will be guaranteed by using the derivative of the polarization curve modelling (Eq. 1) with respect to the current I to analyse the EIS spectra:

$$\frac{dV_{FC}}{dI} = -\frac{R.T}{\alpha.n.F} \cdot \frac{1}{I + I_n} - \frac{R.T}{\beta.n.F} \cdot \frac{1}{I_{lim} - I} - R_{Ohm} = -R_{Act_QS}(I) - R_{Diff_QS}(I) - R_{Ohm} = -R_{QS}(I) \quad \text{Eq. 8}$$

Where $R_{Act_QS}(I)$ and $R_{Diff_QS}(I)$ respectively correspond to activation and diffusion slope contributions to the whole slope of the polarization curve named here $R_{QS}(I)$.

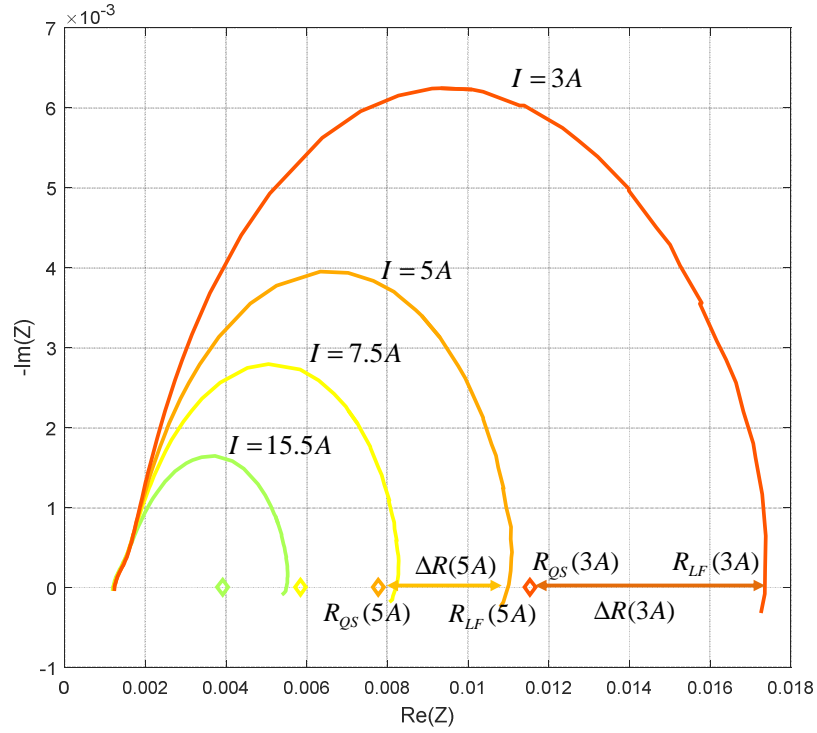
As already said, this relation induces that the EIS measured resistance for the null frequency point $R_{Zero}(I)$ must correspond to the slope value $R_{QS}(I)$ for a given current. Unfortunately, the lowest frequency point available in the EIS measurements is 100 *mHz* (having reliable and repeatable measurements under this frequency is difficult because of the slight fuel cell instability). The exploitation of the EIS measurements leads to introduce a low frequency resistor $R_{LF}(I)$ obtained by extracting the real part of the impedance for the frequency point of 100 *mHz*.

Whatever the polarization current, $R_{LF}(I)$ is such as $R_{LF}(I) > R_{QS}(I)$ for the three tested MEAs. An example is depicted in Fig. 9.a where the values of the polarization slope $R_{QS}(I)$ are positioned on the EIS spectra for several polarization currents for MEA 2. The difference $\Delta R(I)$ between $R_{LF}(I)$ and $R_{QS}(I)$ is plotted as a function of current in Fig. 9.b for all the MEAs.

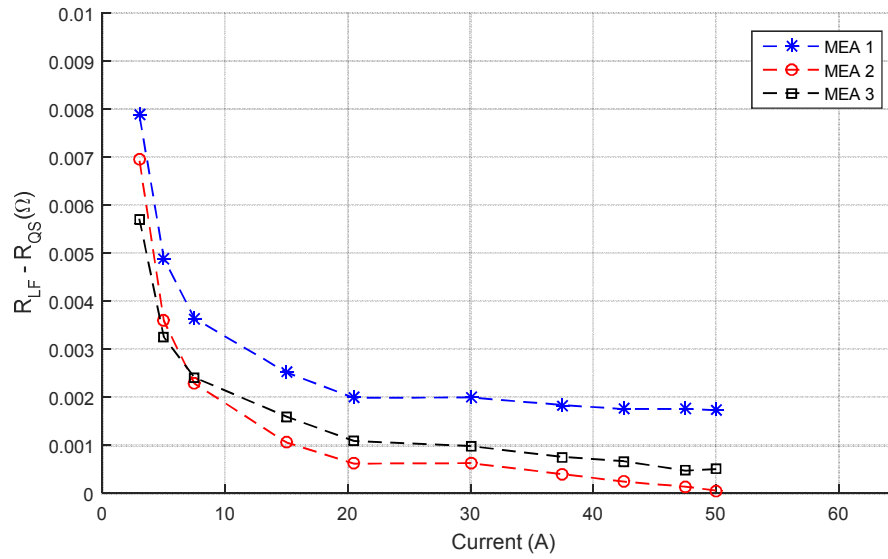
That implies that the FC impedance cannot be modelled using only classical ohmic, activation and diffusion impedances. An additional term Z_{Res} (Res for residual) must be added to take into account this impedance “excess”:

$$Z_{FC}(I) = R_{Ohm} + Z_{Act}(I) + Z_{Diff}(I) + Z_{Res}(I) \quad \text{Eq. 9}$$

In the range [0-100 *mHz*], the term Z_{Res} has to decrease to 0 in order to ensure the correspondence with the slope of the polarization curve but this very low frequency behavior is not concerned in this paper. We can observe in Fig. 9.b that the behaviors in terms of $\Delta R(I)$ for MEA 2 and MEA 3 are quite close; that is quite unexpected as already underlined in part 4.1. Globally, the shapes are the same ones for the three MEAs and seems to be a function of type I/I .



(a)



(b)

Fig. 9. (a) Illustration of the mismatch between quasi static and dynamic behaviors at low frequencies for MEA 2 and (b) the difference $\Delta R(I)$ between $R_{LF}(I)$ and $R_{QS}(I)$ as a function of current for the 3 MEAs

4.3. Analysis of the EIS spectra thanks to the concept of time-constant spectra

For each tested MEA, the objective is to separate the three impedances $Z_{Act}(I)$, $Z_{Diff}(I)$ and $Z_{Res}(I)$ contained in the measured EIS spectra. Each impedance is supposed to be composed of a set of serial RC cells as shown in Fig. 10.

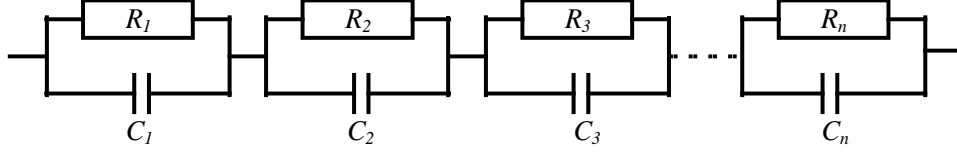


Fig. 10. Equivalent electrical model based on serial RC cells

In association to this serial RC circuit, it is possible to introduce, for an easiest reading and exploitation of the impedances, the concept of time-constant spectrum [8] [24]. In this representation, each RC cell is placed in a $[R; \tau]$ plan where each time constant $\tau_i = R_i \cdot C_i$ (x-axis) is associated to its resistance value R_i (y-axis) as illustrated in Fig. 11.

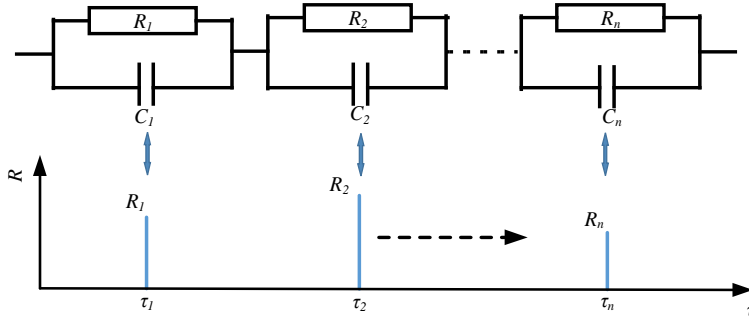


Fig. 11. Time-constant spectrum concept

Using this representation, the purpose is to build an equivalent circuit by distributing the time constants τ_i over a chosen range $[\tau_{min} \dots \tau_{max}]$ and identify the corresponding R_i . Compared to other equivalent electrical approaches, this model has no *a priori* on the number of significant time constants to take into account. The identification process will automatically attribute a “weight” to each τ_i by choosing the appropriate R_i .

A first part of the circuit impedance has N_{Cell_Act} RC cells and is dedicated to model the activation phenomena Z_{Act} . This impedance is built from a set of log-spatially distributed time constants such as $\tau_{Act} = [\tau_{Act_min} \dots \tau_{Act_max}]$. The expression of $R_{Act_QS}(I)$ helps us to impose specific variation laws for activation impedance by making the assumption that both activation resistances and their associated time constants follow the same law as $R_{Act_QS}(I)$. Z_{Act} is then defined using Eq. 10.

$$Z_{Act}(I) = \frac{R.T}{\alpha.n.F} \sum_{k=1}^{N_{Cell_Act}} \frac{\theta_{Act}(k)}{I + I_n} \frac{1}{1 + j.\omega. \frac{\tau_{Act}(k)}{I + I_n}} \quad \text{Eq. 10}$$

Where $\alpha=0.5$ and I_n is the respective value identified in part 3.3.

The authors have to underline here the first way used in this part to ensure the consistency between static and dynamic modelling: in an original way for the time-constant spectra approach, we force our algorithm to find a potential contribution of activation phenomena in EIS measurements by using the derivative of the activation law parameterized for the static model.

Moreover, to force the consistency between polarization curves and EIS measurements in a second way, the low frequency resistance of the activation impedance model must match up with the value of R_{Act_QS} :

$$\frac{R.T}{\alpha.n.F} \sum_{k=1}^{N_{Cell_Act}} \frac{\theta_{Act}(k)}{I + I_n} = R_{Act_QS}(I) \quad \text{Eq. 11}$$

In a similar way, the consistency between static and dynamic modelling is going to be ensured for diffusion phenomena in the following paragraphs.

The second impedance Z_{Diff} has N_{Cell_Diff} RC cells and is dedicated to model the diffusion phenomena. This impedance is built from a set of log-spatially distributed time constants $\tau_{Diff} = [\tau_{Diff_min} \dots \tau_{Diff_max}]$. The expression of $R_{Diff_QS}(I)$ is also used here to impose specific variations laws to the diffusion impedance:

$$Z_{Diff}(I) = \frac{R.T}{\beta.n.F} \sum_{k=1}^{N_{Cell_Diff}} \frac{\theta_{Diff}(k)}{I_{lim} - I} \frac{1}{1 + j.\omega.\frac{\tau_{Diff}(k)}{I_{lim} - I}} \quad \text{Eq. 12}$$

Where β and I_{lim} are the respective values identified in part 3.3.

In the case of diffusion, the consistency between polarization curves and EIS measurements is ensured by Eq. 13.

$$\frac{R.T}{\beta.n.F} \sum_{k=1}^{N_{Cell_Diff}} \frac{\theta_{Diff}(k)}{I_{lim} - I} = R_{Diff_QS}(I) \quad \text{Eq. 13}$$

Finally, the third impedance Z_{Res} has N_{Cell_Res} RC cells and is a residual impedance. It is dedicated to model the impedance part of the EIS which cannot be included in Z_{Diff} and Z_{Act} because of the restrictions on 'null' frequency values imposed by Eq. 9 and Eq. 11. This impedance is built from a set of log-spatially distributed time constants $\tau_{Res} = [\tau_{Res_min} \dots \tau_{Res_max}]$.

$$Z_{Res} = \sum_{k=1}^{N_{Cell_Res}} \frac{\theta_{Res}(k)}{1 + j.\omega.\tau_{Res}(k)} \quad \text{Eq. 14}$$

The final impedance model is then in the form of RC cells subdivided into 3 parts modelling the activation, the diffusion and the residual impedances as shown in Fig. 12. L_{Elec} is the wiring inductance and is considered as unique for all EIS of the same MEA.

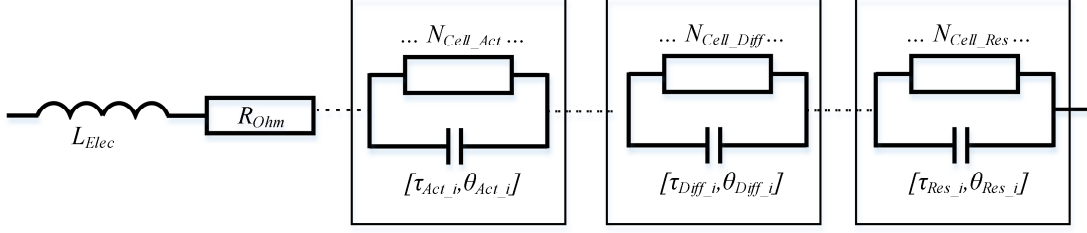


Fig. 12. Final used fuel cell impedance model

It can be noticed that Z_{Act} and Z_{Diff} explicitly depend on the current. So, identifying θ_{Act} and θ_{Diff} implies a complete knowledge of $Z_{Act}(I)$ and $Z_{Diff}(I)$ for all EIS currents. θ_{Act} and θ_{Diff} , having respectively a size of N_{Cell_Act} and N_{Cell_Diff} , are then a part of the final vector to identify θ and are unique for all the polarization currents. As to Z_{Res} , it is necessary to have as much Z_{Res} as EIS because it is different for each EIS. So θ_{Res} is then a parameter vector composed of N_{EIS} sub-vectors of size N_{Cell_Res} .

The experimental data required for the identification process is the complete set of N_{EIS} spectroscopies to take into account the current sensitivity. The final vector θ to identify is shown in Eq. 15:

$$\theta = [\theta_{Act} \quad \theta_{Diff} \quad \theta_{Res_1} \dots \theta_{Res_N_{EIS}} \quad L_{Elec}] \quad \text{Eq. 15}$$

Given that R_{ohm} is directly extracted from the corresponding spectroscopy, it is not included in θ . The objective of the identification problem is to find the parameters θ_i of the circuit by minimizing the difference between the experimental measurement and the impedance model response for both real and imaginary parts of the impedance.

$$\min[J_\theta] = \min \left[\sum_{k=1}^{N_{EIS}} \sum_{i=1}^N (Z_{Model_real_k}(\omega_i) - Z_{EIS_real_k}(\omega_i))^2 + \sum_{k=1}^{N_{EIS}} \sum_{i=1}^N (Z_{Model_imag_k}(\omega_i) - Z_{EIS_imag_k}(\omega_i))^2 \right] \quad \text{Eq. 16}$$

To favor the respect of the polarization curve slope, the optimization criteria take into account Eq. 17, Eq. 18 and Eq. 19.

$$\varepsilon_{Act}(I) = \frac{R.T}{\alpha.n.F} \sum_{k=1}^{N_{Cell_Act}} \frac{\theta_{Act}(k)}{I + I_n} - R_{Act_QS}(I) \quad \text{Eq. 17}$$

$$\varepsilon_{Diff}(I) = \frac{R.T}{\beta.n.F} \sum_{k=1}^{N_{Cell_Diff}} \frac{\theta_{Diff}(k)}{I_{lim} - I} - R_{Diff_QS}(I) \quad \text{Eq. 18}$$

$$\min[J_\theta] = \min \left[\sum_{k=1}^{N_{EIS}} (\varepsilon_{Z_real_k}^2 + \varepsilon_{Z_imag_k}^2) + \sum_{k=1}^{N_{EIS}} (\varepsilon_{Act}^2(k) + \varepsilon_{Diff}^2(k)) \right] \quad \text{Eq. 19}$$

4.4. Results and discussion

Based on the content of the previous section, an identification is carried out via the EIS data ($N_{EIS} = 10$) for each MEA. Fig. 13 shows an example of EIS experimental data of MEA 2 and the model fitted curves. The chosen parameters are: $N_{Cell_Act} = 30$, $N_{Cell_Diff} = 30$, $N_{Cell_Res} = 20$.

It may be noticed that the electrical model fits well the experimental data with a relatively low error (below 1%) on the real and the imaginary Nyquist axes.

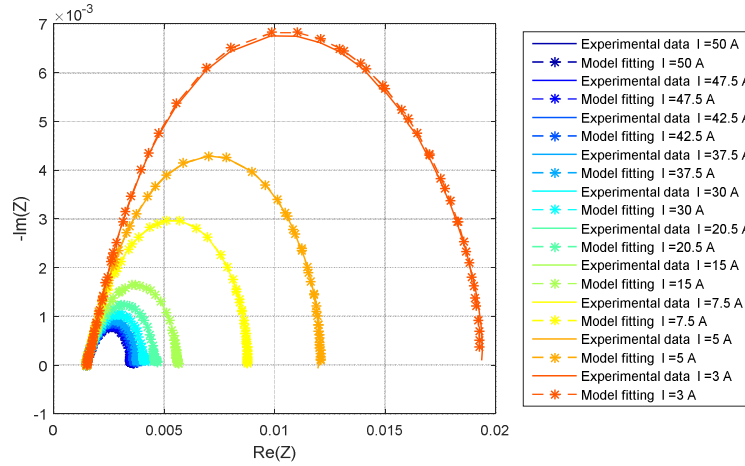


Fig. 13. Experimental data and the model fitting for 10 currents (MEA 2)

In Fig. 14, we can observe a typical result for the three different impedances Z_{Act} (black), Z_{Diff} (magenta), and Z_{Res} (green). The correspondences between R_{Act_QS} , R_{Diff_QS} and the values of impedances Z_{Act} , Z_{Diff} at low frequencies are perfectly obtained as required, ensuring the consistency between the quasi static and dynamic behaviors (small circles in the figure). But, the consequence clearly is that a residual impedance (green) is absolutely necessary to model the remaining part of the impedance after having considered activation and diffusion phenomena in a classical way.

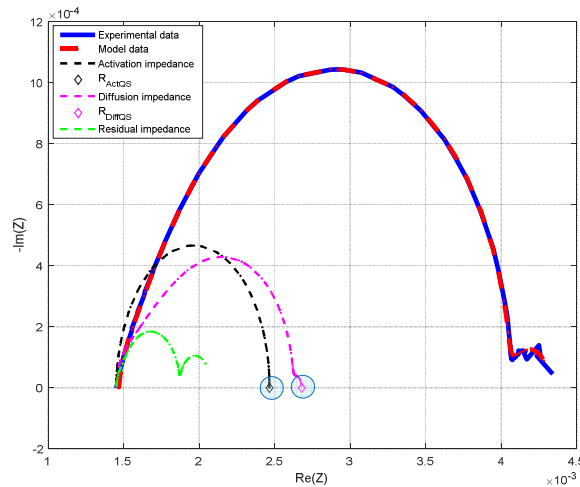


Fig. 14. Experimental data, model data, impedances related to the activation, the diffusion, the residue, and resistances obtained via the slopes of the polarization curve modelling for MEA 2 at $I=30\text{ A}$

To evaluate the method sensitivity with regards to MEA characteristics, the identification results for all the MEAs are compared. The set of components (different membrane thicknesses, different platinum loadings for the active layer) should highlight the impact of each modification in the MEA properties on the obtained time-constant spectra. Typical

results for the 3 MEAs for activation and diffusion time-constant spectra and related Nyquist plots are shown in Fig. 15 and Fig. 16 respectively for a current of 30 A.

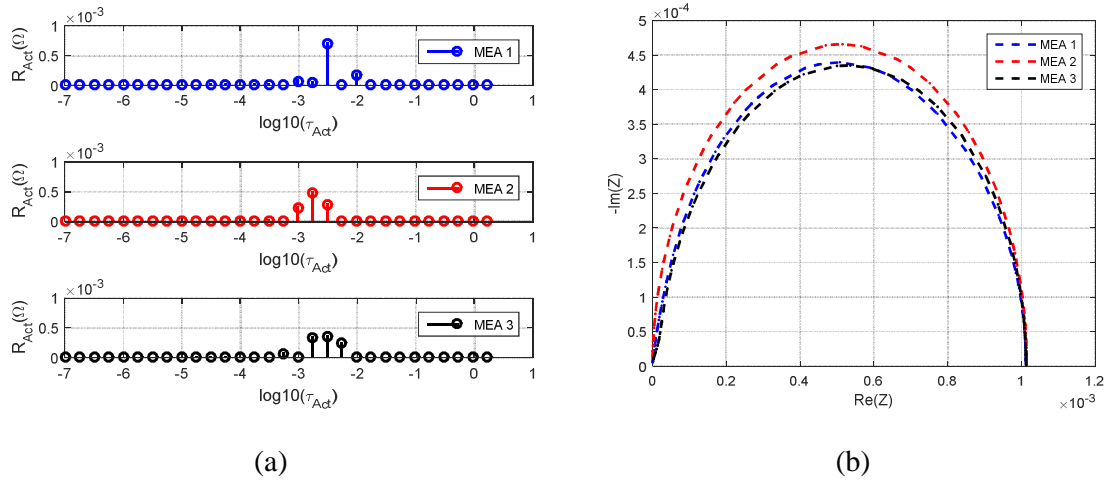


Fig. 15. (a) Activation time-constant spectra for the 3 MEAs for 30 A and (b) Nyquist plots of impedances related to the activation for each MEA at 30 A

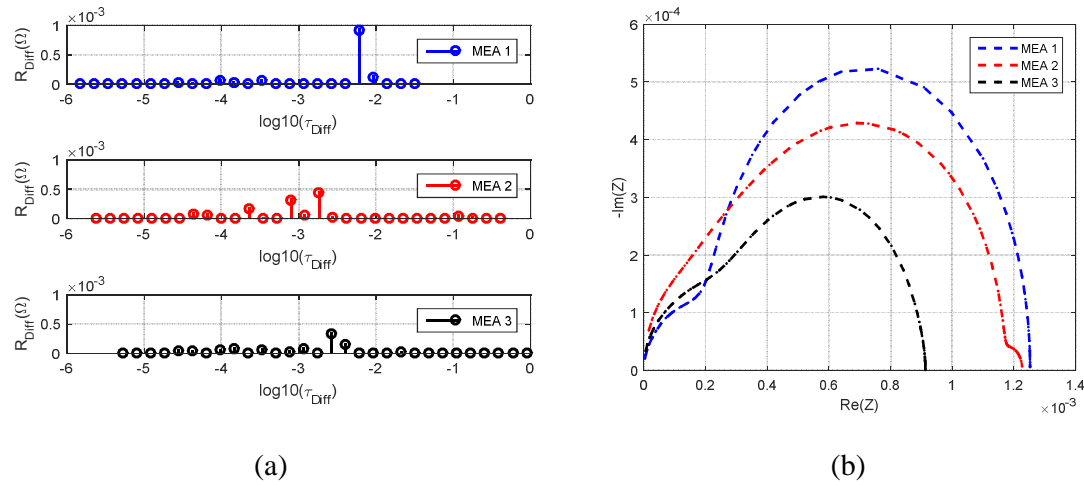


Fig. 16. (a) Diffusion time-constant spectra for the 3 MEAs for 30 A and (b) Nyquist plots of impedances related to the diffusion for each MEA at 30 A

Logically the three MEAs have activation characteristics close to each other: this is mostly visible thanks to Nyquist plots (Fig. 15.b). As Eq. 8 shows it, the activation current I_0 (supposed not to be dependent on the current as classically) is indeed removed by the derivative operation and thus is supposed to not have an effect on the activation impedance. The pseudo diameters of the three pseudo circles are thus mainly linked to the parameter α (the effect of the parameter I_n can be neglected in our case). As $\alpha=0.5$ by assumption for the three MEAs, these three pseudo diameters are logically identical.

The dynamical behaviours for activation phenomena, even if they are close, are sensibly different: this time, this is more easily visible thanks to time-constant spectra (Fig. 15.a). We

can see that the significative time constants for each MEA are different but localized around the same time constants explaining why the three pseudo circles are close (Fig. 15.b).

Let us compare now the three global capacitances (N_{Cell_Act} capacitors in series) given by the Table 4. These global capacitances can be assimilated to the double layer phenomena (C_{dl}) which correspond to spontaneous accumulations of electrical charges with different natures (electrons and ions) at each interface electrode/ membrane. In other words and more exactly, they are supposed to give an image of each interface between each catalyst layer and the membrane. As the reader can imagine this, these interfaces are very complex phenomena.

These global capacitances are approximated assuming that the RC cells in series related to the activation can be assimilated to a unique equivalent RC cell since the shape of the related impedance is close to a “half-circle”. The value of each MEA capacitance is almost similar for all currents. An average value of the global capacitance related to each MEA is shown in Table 4. According to this table, we can see that the global capacitances C_{dl} related to MEA 1 and MEA 3 are higher than that of MEA 2. We can conclude that there is a quite clear correlation between the platinum loadings and the values of these global capacitances.

MEA number	Approximation of C_{dl} (F)
MEA 1	3.04
MEA 2	1.74
MEA 3	2.64

Table 4. Estimated values of the global capacitances C_{dl} for the three MEAs

Concerning the behaviors of the diffusion phenomena illustrated in Fig. 16, they are very clearly different for each MEA. The ranges of time-constants swept are very different as the time-constant spectra illustrate it Fig. 16.a. That justifies the very different shapes of the Nyquist plots in Fig. 16.b. In any case, it appears one more time that diffusion phenomena are difficult to model with a frozen structure in terms of equivalent electrical circuits. This is one of the lessons of our analysis.

Concerning the width of each obtained shape (expanded concept of pseudo diameters), we can recall that it is forced by our approach to be equal to $R_{Diff_QS}(I)$ (given by Eq. 7). That means that each width, at a given current, is fixed by the values of the parameters β and I_{lim} . In Fig. 16.b, we can see that the pseudo diameters of MEA 1 and MEA 2 are very close and larger than that of MEA 3. Fig. 17 shows the evolution according to the current of $R_{Diff_QS}(I)$ (Eq. 8) which is the contribution of the diffusion phenomena to the slope of the polarization curve for the three MEAs. If we look specifically the current of 30 A in Fig. 16, we can find logically and perfectly (again, we have forced the identification resolution in this way!) the ranking of the three MEAs observed in Fig. 16.b and the values of the three diffusion impedances. Fig. 17 illustrates also that for higher currents, the diffusion impedance spectra are going to evolve in a complex way due to the different crossings of three curves. For example, at 60 A, the ranking will be fully changed and the three pseudo diameters will be very different from each other, compared with the behavior at 30 A. That illustrates again all the difficulties to interpret the diffusion phenomena from the dynamical point of view even in small signals as for the EIS.

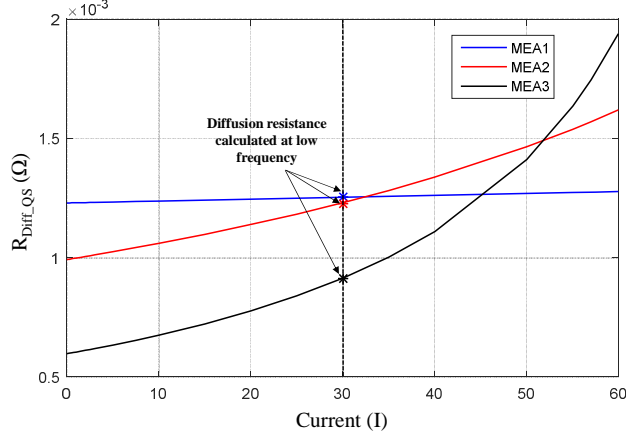


Fig. 17. Evolution according to the current of R_{Diff_QS} for the three MEAs and the three low frequency diffusion resistances related to each MEA at $I= 30 A$ issued from our identification process for the impedance spectra.

4.5. Residual impedance interpretation

The obtained results in terms of spectra and impedances related to the residual part are shown in Fig. 18 for $I= 30 A$. We remind that the residual spectra differ from activation and diffusion spectra because this part of the whole impedance is not constrained by physical laws in opposition to activation and diffusion impedances.

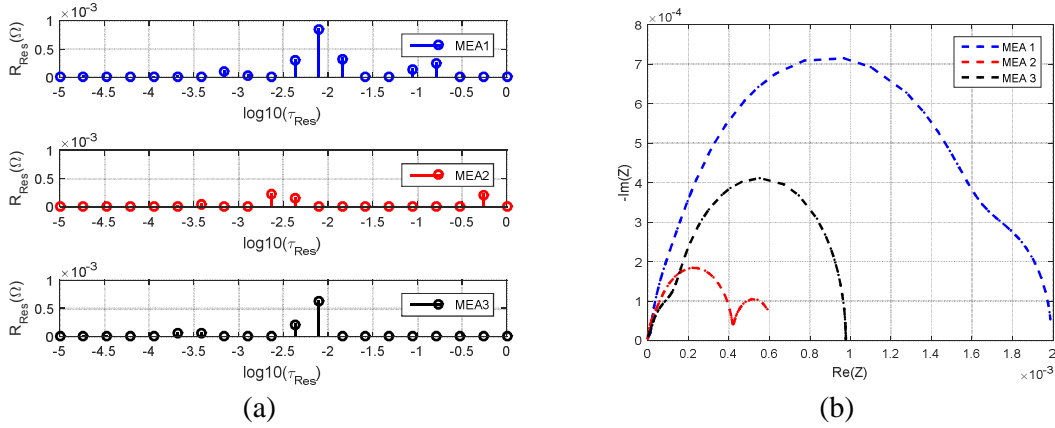


Fig. 18. (a) Residual spectra for the 3 MEAs for 30 A and (b) Nyquist plot of impedances related to the residual for each MEA at 30 A

Observing the residual spectra (in red in Fig. 18.b for MEA 2), we can assume that it is made of two parts: a high frequency part and a low one especially at high currents. An example of the residual impedance spectra is shown in Fig. 19 for each current for MEA 2.

Fig. 19. Evolution of the residual impedance as a function of current for MEA 2

Using the residual time-constant spectrum, we separate the two zones and we draw the impedances corresponding to each zone in Nyquist plot. The idea consists in the separation of time-constant spectra related to high and low frequencies, and then in reconstructing each impedance zone in Nyquist plot via its spectra. An example of this process is applied to MEA 2 at $I=30\text{ A}$ and shown in Fig. 20 and Fig. 21.

Fig. 20. Separation of the high frequency zone (named Res 1) and low frequency zone (named Res 2) applied to the time-constant spectrum of MEA 2 at $I=30\text{ A}$

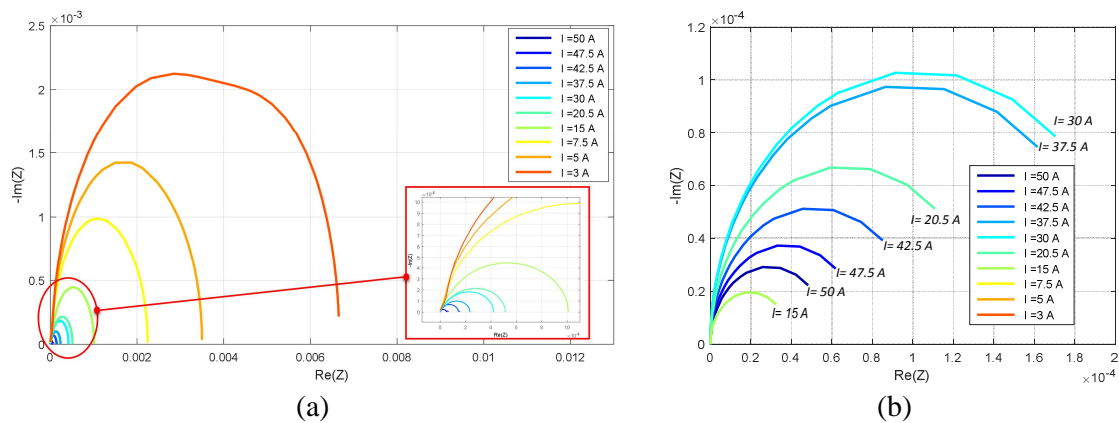


Fig. 21. Evolution of the residual impedance for (a) the high frequency impedance zone (Res 1) and (b) the low frequency impedance zone (Res 2) for MEA 2

The impedance of the first zone (Res 1) clearly varies inversely with the current contrarily to the impedance of the second zone (Res 2) which has a very different progression with the current. To properly explain this trend, we have drawn the evolution of the resistance

calculated at low frequency for each part of the residual as a function of current in Fig. 22. Res 2 has a “bell” shape in terms of evolution.

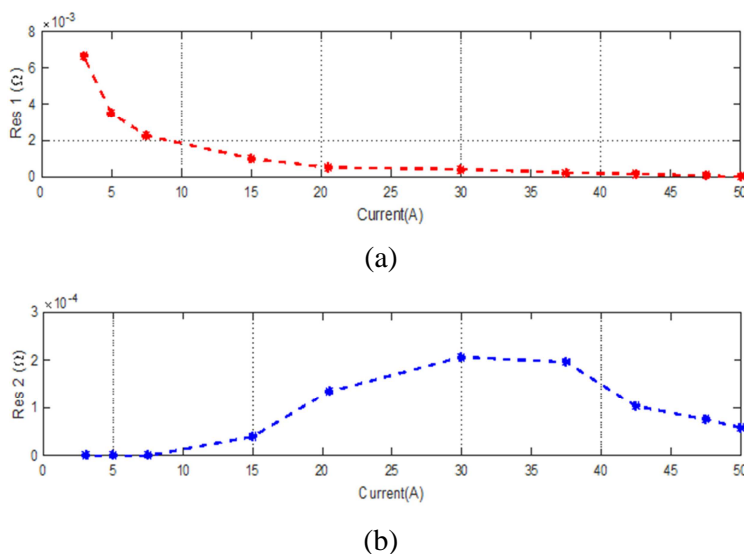


Fig. 22. Evolution of the resistance calculated at low frequency for (a) Res 1 and (b) Res 2 as a function of current for MEA 2

The first residual part Res 1 could be explained by the platinum oxidation. This evolution according to the current is similar to that of the activation resistance $R_{Act_QS}(I)$ (Eq. 8). That would plead in favor of the assumption of the influence of platinum oxidation on the activation phenomena at low frequencies. Even if highly probably complex, this link seems logical: the activation phenomena depend on the active surface of platinum (see Fig. 6 and associated comments) and the platinum oxidation modifies the active surface according to the current. Future modelling works have to be *a priori* oriented in this way: Res 1 and activation impedance are not two different phenomena but coupled phenomena.

The Res 2 is more complex to analyze. It is now clear that the EIS is not noninvasive at low frequencies in terms of fluidic operation for the fuel cell. Gas oscillations in channels can be created by imposed low frequency current oscillations (unavoidable by principle of the EIS) generating a certain impedance [25] [6] [26]. Interactions with the regulation of gases at low frequency cannot be also excluded, not to say very probable; and, each test bench has its proper settings for gas regulation. In the same way as for activation phenomena, these fluidic phenomena appearing at low frequencies could be seen in future works as an extension of diffusion phenomena considered in a classical way in this paper.

Up to now, the spectra and impedances corresponding to the residual part cannot be used, with our current knowledge level, to determine more model parameters but offer promising prospects to explain some phenomena that appear at low frequencies. More improvements could be added, especially concerning the way how we separate actually Res 1 and Res 2 according to the frequency range. Introducing an identification process integrating particular laws could be a reasonable alternative to analyze the residual.

To conclude this part, our modelling approach points out that this residual impedance is necessary to properly describe the dynamic phenomena in a FC but up until now, interpreting its physical signification remains an issue to be addressed.

5. Conclusion

In this study, an identification process fed by experimental data, especially the polarization curve and the EIS, allows to find parameters of both a quasi-static model and a dynamic model describing the phenomena involved in the fuel cell operation. The proposed models were built through specific physicochemical laws, such as activation and diffusion.

The exploitation of EIS has been performed by introducing an original electrical equivalent circuit to separate the activation and diffusion phenomena in accordance to the polarization curve slopes. In this model, impedances related to activation and diffusion are constrained to match the quasi static measurements of the polarization curves. As a consequence, it has been shown that introducing a specific residual impedance in addition to diffusion and activation impedances is necessary to properly model the EIS of a fuel cell.

Several MEAs have been tested and compared to demonstrate that the proposed approach got sensitiveness to constitutive elements of the fuel cell such as membrane thickness and platinum loading. Concerning the quasi static point of view, the results show that identifying the polarization curves provides interesting and consistent results with regards to activation and crossover currents under some conditions: $\alpha=0.5$ and R_{ohm} estimated via EIS. Identified parameters have been compared to cyclic voltammetry measurements to attest the validity of the results.

Concerning the dynamic point of view, the exploitation of the time-constant spectra remains uncompleted but permitted us to advance. Activation and diffusion contributions are *a priori* the clearest ones to extract from the impedance spectra but additional experiments must be performed to verify their sensitivity to other intrinsic characteristics such as gas diffusion channel geometry or extrinsic characteristics such as gas feeding, stoichiometry, relative humidity... **Our results confirm that it is difficult to model and to interpret diffusion phenomena in a simple and fixed way in terms of model.** We are **moreover** convinced that **relevant** information is also embedded into the residual impedance, but its exploitation is still an issue. The main prospects for that specific point are to link this impedance to the oxidation of platinum and to gas channel oscillations. Adding diversity in the fuel cell characteristics and solicitations for future tests could help us to understand mechanisms involved by studying their impact on the different spectra.

This article was focused on the ability of the proposed method to properly interpret through modelling the typical characterization of a fuel cell along its lifetime, i.e. V-I curves and EIS along them. We can imagine easily applying this method for ageing campaigns with scheduled characterizations (in real applications, during maintenance phases for example). To adapt this approach for real time applications, additional researches have to be performed to optimize the measurements (during, for example, specific phases of the mission profile or during start/stop phases).

So far, our objective with this kind of methods is not to have real time corrective actions on fuel cell control but only to obtain periodical information about the fuel cell state of health (for example to forecast a maintenance). Our methodology is suitable to follow slow degradations, thus we don't have any constraints about time computation.

Acknowledgments

This study was conducted as a part of the Fuel Cell Hydrogen in Aeronautic applications (FUCHYA) project led by the Institute of Technological Research Saint Exupéry (Institut de Recherche Technologique IRT Saint Exupéry) under a contract with Laplace laboratory,

Zodiac Aerospace, Safran Power Units, and Airbus Group. The authors would like to thank all the project members for their technical assistance and discussions.

References

- [1] E. Cho, "A Study on Performance Degradation of PEMFC by Water Freezing," *J Electrochem Soc*, vol. 150, no. 12, pp. A1667–A1670, 2003.
- [2] W. Mérida, D. A. Harrington, J. M. Le Canut, and G. McLean, "Characterisation of proton exchange membrane fuel cell (PEMFC) failures via electrochemical impedance spectroscopy," *J. Power Sources*, vol. 161, no. 1, pp. 264–274, Oct. 2006.
- [3] G. Mousa, J. DeVaal, and F. Golnaraghi, "Diagnosis of hydrogen crossover and emission in proton exchange membrane fuel cells," *Int. J. Hydrog. Energy*, vol. 39, no. 36, pp. 21154–21164, Dec. 2014.
- [4] G. Mousa, F. Golnaraghi, J. DeVaal, and A. Young, "Detecting proton exchange membrane fuel cell hydrogen leak using electrochemical impedance spectroscopy method," *J. Power Sources*, vol. 246, pp. 110–116, Jan. 2014.
- [5] M. Chandesris, C. Robin, M. Gerard, and Y. Bultel, "Investigation of the difference between the low frequency limit of the impedance spectrum and the slope of the polarization curve," *Electrochimica Acta*, vol. 180, pp. 581–590, Oct. 2015.
- [6] I. A. Schneider, D. Kramer, A. Wokaun, and G. G. Scherer, "Oscillations in Gas Channels," *J. Electrochem. Soc.*, vol. 154, no. 8, p. B770, 2007.
- [7] S. K. Roy, M. E. Orazem, and B. Tribollet, "Interpretation of Low-Frequency Inductive Loops in PEM Fuel Cells," *J. Electrochem. Soc.*, vol. 154, no. 12, p. B1378, 2007.
- [8] T. Génévé, J. Régnier, and C. Turpin, "Fuel cell flooding diagnosis based on time-constant spectrum analysis," *Int. J. Hydrog. Energy*, vol. 41, no. 1, pp. 516–523, Jan. 2016.
- [9] M. A. Travassos, V. V. Lopes, R. A. Silva, A. Q. Novais, and C. M. Rangel, "Assessing cell polarity reversal degradation phenomena in PEM fuel cells by electrochemical impedance spectroscopy," *Int. J. Hydrog. Energy*, vol. 38, no. 18, pp. 7684–7696, Jun. 2013.
- [10] A. Szalai and V. Székely, "Distributed RC One-Ports: Characteristic Functions and Their Relations," *Period. Polytech. Electr. Eng. Comput. Sci.*, vol. 60, no. 3, pp. 178–186, 2016.
- [11] V. Székely, "On the representation of infinite-length distributed RC one-ports," *IEEE Trans. Circuits Syst.*, vol. 38, no. 7, pp. 711–719, 1991.
- [12] V. Székely, "Identification of RC networks by deconvolution: chances and limits," *IEEE Trans. Circuits Syst. Fundam. Theory Appl.*, vol. 45, no. 3, pp. 244–258, 1998.
- [13] "PaxiTech, fuel cell, welcome on the PaxiTech's website." [Online]. Available: <http://www.paxitech.com/>. [Accessed: 18-May-2017].
- [14] D. Baker, W. Gu, Y. Liu, and M. Mathias, "Tutorial: Frontiers in Application of Impedance Diagnostics to H₂-Fed Polymer Electrolyte Fuel Cells," in *Meeting Abstracts*, 2008, pp. 914–914.

- [15] X. changjun and Q. shuhai, "Drawing impedance spectroscopy for Fuel Cell by EIS," *Procedia Environ. Sci.*, vol. 11, pp. 589–596, 2011.
- [16] G. Fontes, C. Turpin, S. Astier, and T. A. Meynard, "Interactions Between Fuel Cells and Power Converters: Influence of Current Harmonics on a Fuel Cell Stack," *IEEE Trans. Power Electron.*, vol. 22, no. 2, pp. 670–678, Mar. 2007.
- [17] A. Pessot *et al.*, "Contribution to the modelling of a low temperature pem fuel cell in aeronautical conditions by design of experiments," *Math. Comput. Simul.*, Aug. 2018.
- [18] M. Aghighi, M. A. Hoeh, W. Lehnert, G. Merle, and J. Gostick, "Simulation of a full fuel cell membrane electrode assembly using pore network modeling," *J. Electrochem. Soc.*, vol. 163, no. 5, pp. F384–F392, 2016.
- [19] K. C. Neyerlin, W. Gu, J. Jorne, and H. A. Gasteiger, "Determination of Catalyst Unique Parameters for the Oxygen Reduction Reaction in a PEMFC," *J. Electrochem. Soc.*, vol. 153, no. 10, p. A1955, 2006.
- [20] T. Génové, "Méthodes de diagnostic des piles à combustible," Doctoral thesis, Institut Nationale Polytechnique de Toulouse INPT, 2016.
- [21] E. Brightman, G. Hinds, and R. O'Malley, "In situ measurement of active catalyst surface area in fuel cell stacks," *J. Power Sources*, vol. 242, pp. 244–254, Nov. 2013.
- [22] K.-S. Lee *et al.*, "Development of a galvanostatic analysis technique as an in-situ diagnostic tool for PEMFC single cells and stacks," *Int. J. Hydrog. Energy*, vol. 37, no. 7, pp. 5891–5900, Apr. 2012.
- [23] C. Turpin and A. Rakotondrainibe, "Method of Characterizing an Electrical System by Impedance Spectroscopy," WO/2010/097354, 03-Sep-2010.
- [24] T. H. Wan, M. Saccoccio, C. Chen, and F. Ciucci, "Influence of the Discretization Methods on the Distribution of Relaxation Times Deconvolution: Implementing Radial Basis Functions with DRTtools," *Electrochimica Acta*, vol. 184, pp. 483–499, Dec. 2015.
- [25] I. A. Schneider, S. A. Freunberger, D. Kramer, A. Wokaun, and G. G. Scherer, "Oscillations in Gas Channels," *J. Electrochem. Soc.*, vol. 154, no. 4, p. B383, 2007.
- [26] S. Chevalier, D. Trichet, B. Auvity, J. C. Olivier, C. Josset, and M. Machmoum, "Multiphysics DC and AC models of a PEMFC for the detection of degraded cell parameters," *Int. J. Hydrog. Energy*, vol. 38, no. 26, pp. 11609–11618, Aug. 2013.